nature medicine

Cyclophilin D deficiency attenuates mitochondrial and neuronal perturbation and ameliorates learning and memory in Alzheimer's disease

Heng Du[1], Lan Guo[1], Fang Fang[1], Doris Chen[1], Alexander A Sosunov[2], Guy M McKhann[2], Yilin Yan[3], Chunyu Wang[3], Hong Zhang[4,5], Jeffery D Molkentin[6], Frank J Gunn-Moore[7], Jean Paul Vonsattel[4], Ottavio Arancio[4,5], John Xi Chen[8] & Shi Du Yan[1,4,5]

Cyclophilin D (CypD, encoded by *Ppif*) is an integral part of the mitochondrial permeability transition pore, whose opening leads to cell death. Here we show that interaction of CypD with mitochondrial amyloid-β protein (Aβ) potentiates mitochondrial, neuronal and synaptic stress. The CypD-deficient cortical mitochondria are resistant to Aβ- and Ca^{2+}-induced mitochondrial swelling and permeability transition. Additionally, they have an increased calcium buffering capacity and generate fewer mitochondrial reactive oxygen species. Furthermore, the absence of CypD protects neurons from Aβ- and oxidative stress–induced cell death. Notably, CypD deficiency substantially improves learning and memory and synaptic function in an Alzheimer's disease mouse model and alleviates Aβ-mediated reduction of long-term potentiation. Thus, the CypD-mediated mitochondrial permeability transition pore is directly linked to the cellular and synaptic perturbations observed in the pathogenesis of Alzheimer's disease. Blockade of CypD may be a therapeutic strategy in Alzheimer's disease.

Mitochondrial dysfunction is a feature of the Alzheimer's disease brain[1–5]. Recent studies have highlighted the role of mitochondrial Aβ in Alzheimer's disease pathogenesis[6–15]. Aβ species have been found in the mitochondria of both Alzheimer's disease brain and transgenic mouse models of Alzheimer's disease overexpressing Aβ[6,7,9,13–16]. Accumulation of Aβ in mitochondria occurs before extracellular amyloid deposition and increases with age. Accordingly, Aβ is linked to the mitochondrial malfunction observed in the Alzheimer's disease brain and mouse models of Alzheimer's disease[6,7,17]. For instance, increased expression of amyloid-binding alcohol dehydrogenase, an intracellular Aβ-binding protein, exacerbates Aβ-mediated mitochondrial and neuronal stress[8,9]. Aβ can also directly disrupt mitochondrial function, and such disruption causes oxidative stress[4,18]. However, the essential intracellular mechanisms underlying Aβ-mediated mitochondrial malfunction have yet to be elucidated.

The mitochondrial permeability transition pore (mPTP) has a central role in both necrotic and apoptotic neuronal cell death. Opening of the mPTP collapses the membrane potential and amplifies apoptotic mechanisms by releasing proteins with apoptogenic potential from the inner membrane space[19–21]. The mPTP is thought to involve the voltage-dependent anion channel in the outer membrane, the adenine nucleotide translocase in the inner membrane and CypD in the mitochondrial matrix[20,22–25]. CypD, a peptidylprolyl isomerase F, resides in the mitochondrial matrix and associates with the inner mitochondrial membrane during the opening of the mPTP. Oxidative and other cellular stresses promote CypD translocation to the inner membrane[26–31], and this translocation acts as a key factor to trigger the opening of the mPTP. Moreover, recent studies show that a genetic deficiency in CypD protects from Ca^{2+}- and oxidative stress–induced cell death and that CypD functions as a necessary component of the mPTP[30,32–34]. The observations that Aβ progressively accumulates in brain mitochondria from individuals with Alzheimer's disease and Alzheimer's disease model mice and that oxidative stress is enhanced in an Aβ-rich environment led us to explore the mechanisms underlying Aβ-mediated mitochondrial dysfunction. Our present study offers new insights into the mechanism underlying CypD-dependent mPTP opening and synaptic function during the pathogenesis of Alzheimer's disease.

[1]Departments of Surgery and [2]Neurosurgery, College of Physicians and Surgeons, Columbia University, 630 West 168th Street, New York, New York 10032, USA. [3]Biology Department, Center for Biotechnology and Interdisciplinary Studies, Rensselaer Polytechnic Institute, 110 8th Street, Troy, New York 12180-3590, USA. [4]Department of Pathology and [5]Taub Institute for Research on Alzheimer's Disease and the Aging Brain, College of Physicians and Surgeons, Columbia University, 630 West 168th Street, New York, New York 10032, USA. [6]Department of Pediatrics, University of Cincinnati, Children's Hospital Medical Center, 3333 Burnet Avenue, Cincinnati, Ohio 45229, USA. [7]School of Biology, 79 North Street, University of St. Andrews, St. Andrews KY16 9TS, Scotland. [8]Department of Neurology, Memorial Sloan-Kettering Cancer Center, Cornell University, 1275 York Avenue, New York, New York 10065, USA. Correspondence should be addressed to S.D.Y. (sdy1@columbia.edu).

Received 4 January; accepted 25 August; published online 21 September 2008; doi:10.1038/nm.1868

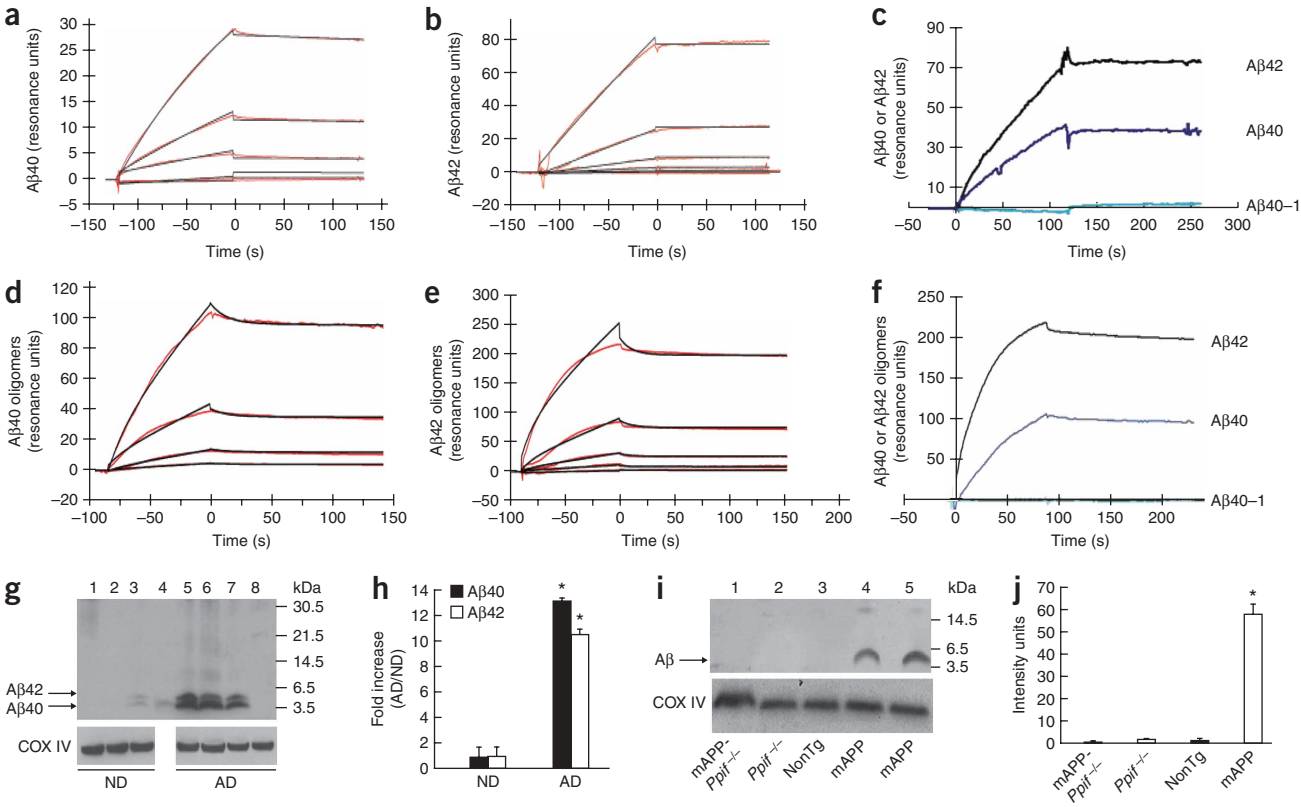

Figure 1 Interaction of CypD with Aβ. (**a**–**f**) Surface plasmon resonance (SPR) analysis of CypD-Aβ interaction. Globally fit data (black lines) were overlaid with experimental data (red lines). (**a**,**b**) Sensorgram of Aβ40 (**a**) or Aβ42 (**b**) interaction with CypD immobilized on the CM5 chip. (**c**) CypD interaction with different types of Aβ. Aβ42 (20 μM), Aβ40 (60 μM) and sequence-reversed Aβ40 (60 μM) bind to CypD immobilized on the CM5 chip. (**d**,**e**) Sensorgram of CypD interaction with oligomers of Aβ40 (**d**) or Aβ42 (**e**) immobilized on the CM5 chip. (**f**) CypD interaction with different types of oligomeric and reversed Aβ immobilized on the CM5 chip. (**g**–**j**) Coimmunoprecipitation of CypD and Aβ in brain mitochondria from human subjects with Alzheimer's disease and transgenic mice. Representative immunoblots show the presence of CypD-Aβ complex in temporal cortical mitochondria of subjects with Alzheimer's disease (AD) or subjects without Alzheimer's disease (ND) (**g**) and in the cortical mitochondria of transgenic mice at 12 months of age (**i**). Lower panels of **g** and **i** indicate immunoblotting of the same preparations of mitochondria with antibody to COX IV, showing equal amount of mitochondrial protein used in the experiment. Lane 4 in panel **g** is an immunoblot for Aβ40 peptide (5 ng). (**h**,**j**) Densitometry of all immunoreactive bands generated from coimmunoprecipitation results (AD, $n = 9$; ND, $n = 6$; transgenic mice, $n = 4$–6 per group). $^*P < 0.0001$ compared to ND or other groups of mice. NonTg, nontransgenic.

RESULTS

Interaction of CypD with mitochondrial Aβ

In view of the increased expression of CypD associated with amyloid pathology in addition to aging (**Supplementary Fig. 1a–i** online), we explored whether CypD serves as a mitochondrial target potentiating Aβ-induced cellular perturbation. We first examined the interaction of CypD with Aβ by surface plasmon resonance (SPR)[35,36]. Recombinant human CypD protein (**Supplementary Fig. 2a** online) bound Aβ in a dose-dependent manner (**Fig. 1a–f**). The CypD-Aβ interaction was specific, because reversed-sequence Aβ peptide showed no binding with CypD (**Fig. 1c**,**f**), and antibodies against either Aβ or CypD inhibited binding (data not shown). The equilibrium dissociation constants (K_d) for Aβ40 (Aβ peptide residues 1–40), Aβ42 (Aβ peptide residues 1–42), oligomeric Aβ40 and oligomeric Aβ42 were 1.7 μM, 164 nM, 227 nM and 4 nM, respectively. Therefore, Aβ oligomers and Aβ42 have higher affinity for binding to CypD.

To determine whether CypD and Aβ actually interact in pathophysiologically relevant settings, we subjected mitochondrial proteins to immunoprecipitation with an antibody to CypD followed by immunoblotting with an antibody to Aβ. CypD-Aβ complexes, corresponding to Aβ-immunoreactive bands, were detected in the cortical mitochondria of Alzheimer's disease brains (**Fig. 1g**) but not (or very little) in those of non–Alzheimer's disease control brains (**Fig. 1g**). Aβ-immunoreactive bands disappeared when the antibody to CypD was replaced by preimmune IgG (**Fig. 1g**). Densitometry of all immunoreactive bands combined revealed that CypD-Aβ complexes were increased by 10–13-fold in Alzheimer's disease cortical mitochondria compared to non–Alzheimer's disease cortical mitochondria (**Fig. 1h**). In parallel, mitochondrial Aβ was increased by nine- to tenfold in Alzheimer's disease brain (**Supplementary Fig. 2b**), indicating an association between CypD-Aβ complex and the presence of mitochondrial Aβ. Furthermore, CypD-Aβ complex was also found in the cortical mitochondria of transgenic mAPP mice overexpressing a mutant form of human amyloid precursor protein (APP) and Aβ, but not in mitochondria from CypD-deficient mAPP mice (mAPP-*Ppif*$^{-/-}$), CypD-null (*Ppif*$^{-/-}$) or nontransgenic mice (**Fig. 1i–j**). Transgenic CypD-null mice are described in **Supplementary Figure 2c–g**. These results indicate that the CypD-Aβ interaction occurs in Alzheimer's disease brain and transgenic mice with Alzheimer's-like pathology.

Confocal and electron microscopic studies confirmed colocalization of CypD and Aβ in mitochondria (**Fig. 2a–d**). In the cerebral cortices

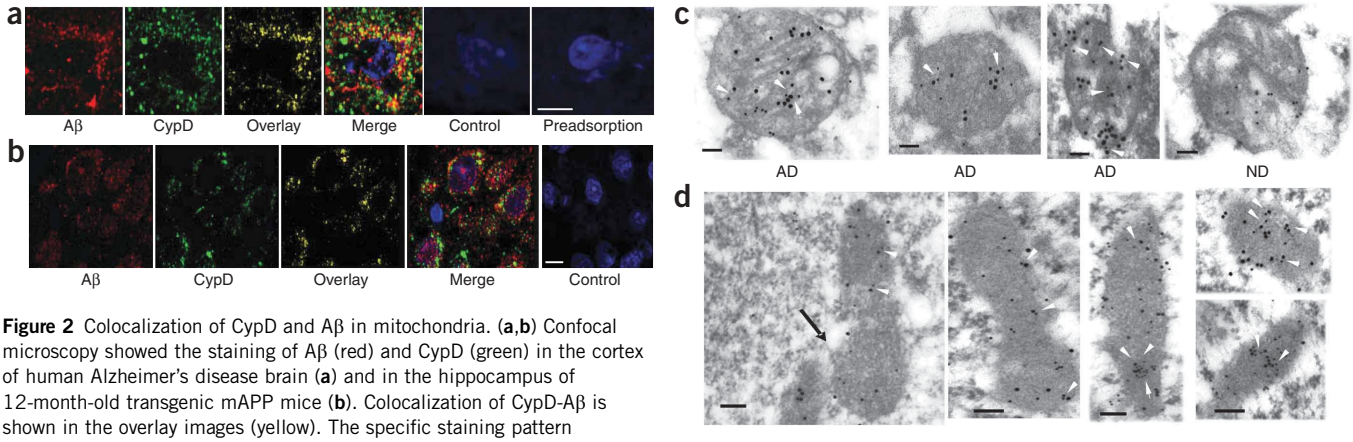

Figure 2 Colocalization of CypD and Aβ in mitochondria. (**a**,**b**) Confocal microscopy showed the staining of Aβ (red) and CypD (green) in the cortex of human Alzheimer's disease brain (**a**) and in the hippocampus of 12-month-old transgenic mAPP mice (**b**). Colocalization of CypD-Aβ is shown in the overlay images (yellow). The specific staining pattern disappeared when the primary antibodies to CypD and Aβ were omitted (control) or preadsorbed with their antigens (CypD protein and Aβ peptide; in **a**). Scale bars, 10 μm for **a** and 5 μm for **b**. (**c**,**d**) Electron microscopy with the double immunogold staining of CypD (12-nm gold particle) and Aβ (18-nm gold particle) showing colocalization of CypD and Aβ in mitochondria of the brains from people with Alzheimer's disease (**c**) and mAPP mice (**d**). Age-matched ND controls show only immunogold particles for CypD (12 nm). Black arrow indicates mitochondria, and white arrowheads denote colocalization of gold particles labeling both CypD and Aβ. Scale bars, 180 nm for **c** and 100 nm for **d**.

of people with Alzheimer's disease (**Fig. 2a**) and mAPP mice (**Fig. 2b**), Aβ and CypD colocalized extensively (**Fig. 2a**,**b**). In the absence of antibodies to Aβ and CypD (**Fig. 2a**,**b**) or after neutralization of the antibodies with their antigens (Aβ42 and CypD protein; **Fig. 2a** and data not shown), staining was lost. Immunogold electron microscopy with gold-conjugated antibodies to Aβ42 (18-nm gold particles) and CypD (12-nm gold particles) revealed that the two different sizes of gold particles were colocalized in the Alzheimer's disease (**Fig. 2c** and **Supplementary Fig. 3a** online) and mAPP brain mitochondria (**Fig. 2d**). Two gold particles that did not overlap but were extremely close to each other may also be indicative of CypD-Aβ colocalization because of the intercenter distance of the two gold particles[37]. As a positive control, we looked for Aβ in the plaques of mAPP mice (**Supplementary Fig. 3g**). The gold particle labeling disappeared when antibodies to Aβ42 and CypD were absent, replaced by preimmune IgG or preadsorbed with the respective antigens (Aβ42 or CypD) (**Supplementary Fig. 3c–f**,**h**,**i**).

CypD deficiency attenuates Aβ-induced mitochondrial stress

First, we assessed the capacity of cortical mitochondria for Ca^{2+} uptake by measuring the disappearance of extramitochondrial free Ca^{2+} from the medium after the addition of $CaCl_2$ pulses. The capacity for calcium uptake changed in an age-dependent manner in both nontransgenic and mAPP mice. Compared to mitochondria from mice at 3–6 months of age, nontransgenic mitochondria from 12-month-old mice showed a trend toward a reduction of the

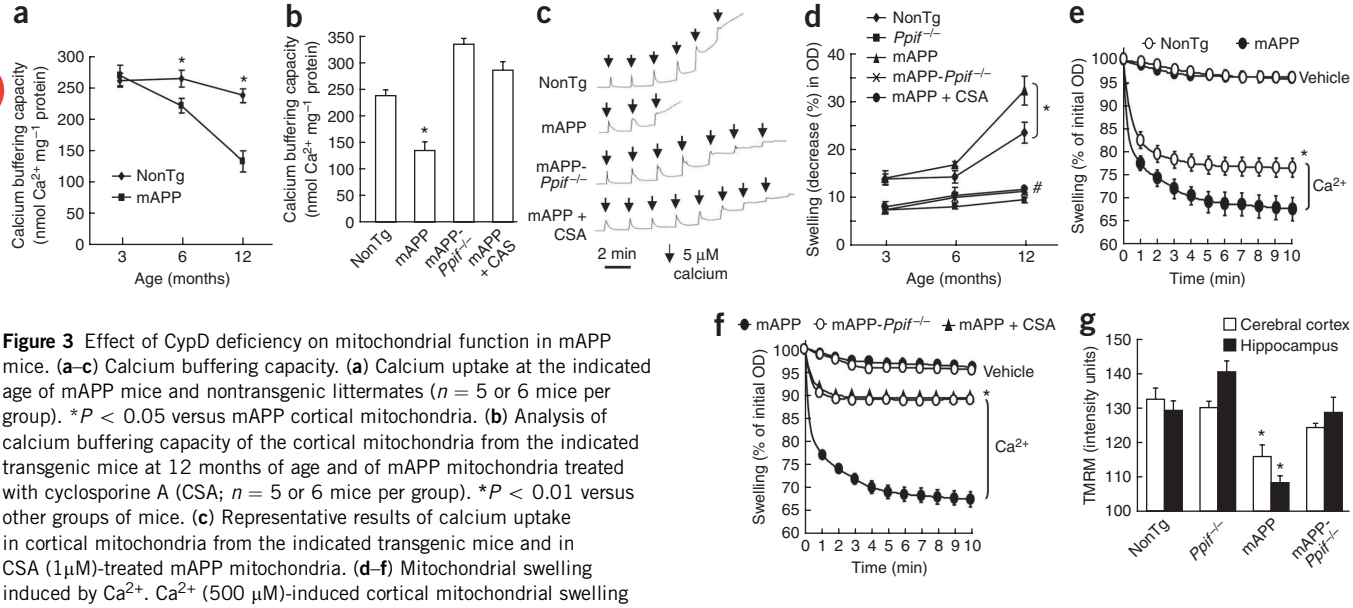

Figure 3 Effect of CypD deficiency on mitochondrial function in mAPP mice. (**a**–**c**) Calcium buffering capacity. (**a**) Calcium uptake at the indicated age of mAPP mice and nontransgenic littermates ($n = 5$ or 6 mice per group). $^*P < 0.05$ versus mAPP cortical mitochondria. (**b**) Analysis of calcium buffering capacity of the cortical mitochondria from the indicated transgenic mice at 12 months of age and of mAPP mitochondria treated with cyclosporine A (CSA; $n = 5$ or 6 mice per group). $^*P < 0.01$ versus other groups of mice. (**c**) Representative results of calcium uptake in cortical mitochondria from the indicated transgenic mice and in CSA (1μM)-treated mAPP mitochondria. (**d**–**f**) Mitochondrial swelling induced by Ca^{2+}. Ca^{2+} (500 μM)-induced cortical mitochondrial swelling was measured in the indicated mice at 3, 6 and 12 months of age, expressed as percentage decrease in the initial optical density (OD) at an absorbance of 540 nm (**d**). Representative results of swelling from the indicated mouse cortical mitochondria (12 months old) or in CSA (1 μM)-treated mAPP mitochondria (**e**,**f**). Data are shown as the percentage change relative to the initial OD at an absorbance of 540 nm. $^*P < 0.05$ versus mAPP mitochondria and $^{\#}P < 0.05$ versus nontransgenic mitochondria. (**g**) The quantification of the intensity of TMRM staining in the indicated mouse brain slices ($n = 4$–6 per group, 12 months old). $^*P < 0.01$ versus nontransgenic and mAPP-*Ppif*$^{-/-}$ mice.

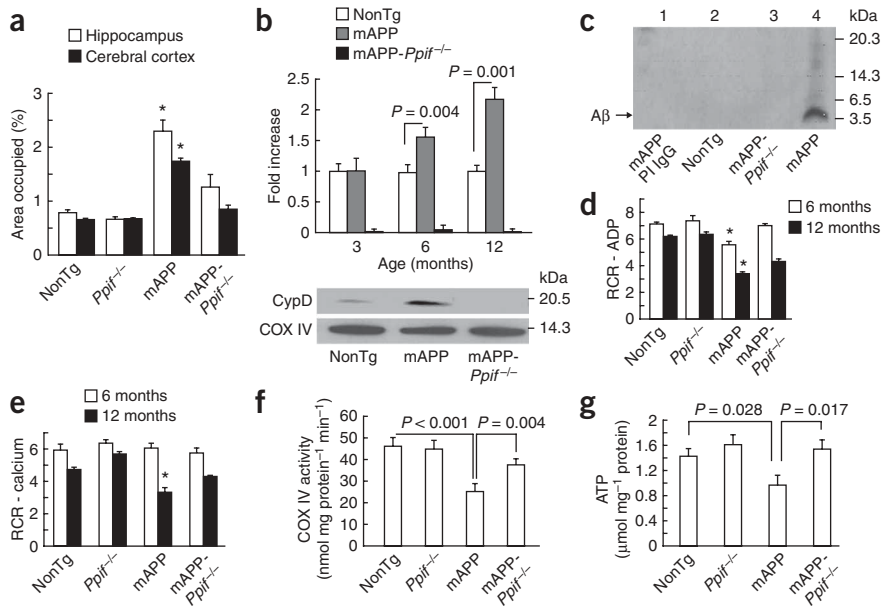

Figure 4 Effect of CypD deficiency on ROS production and mitochondrial function in mAPP mice. (**a**) MitoSox Red staining in mouse brains at 12 months of age. The percentage of area occupied by MitoSox Red staining in the cerebral cortex and hippocampus (CA1 to CA3 regions; $n = 3$ or 4 mice per group, $^*P < 0.001$ versus other groups of mice). (**b**) Immunoblotting of the mitochondrial inner membranes from the indicated mice for CypD. The graph shows densitometry of CypD intensity from all immunoreactive CypD bands combined from the indicated mice. The bottom shows the representative immunoblotting for CypD and COX IV from 12-month-old mice. COX IV served as a control, indicating equal amounts of mitochondrial protein used for the experiment. (**c**) Immunoprecipitation with antibody to CypD followed by antibody to Aβ (6E10) detected an immunoreactive Aβ band in the mitochondrial inner membranes of the indicated mice. The Aβ-immunoreactive band disappeared when antibody to CypD was replaced by the preimmune IgG (lane 1). (**d**–**g**) Respiratory control rate (RCR) in response to ADP (**d**), respiratory control rate in response to Ca^{2+} (**e**), COX IV activity (**f**) and ATP abundance (**g**) in cortices of the indicated mice (12 months old, $n = 8$–10 mice per group). $^*P < 0.05$ versus nontransgenic and mAPP-*Ppif*$^{-/-}$ mice.

capacity for Ca^{2+} uptake (9% reduction, 235.7 ± 10.08 nmoles Ca^{2+} per milligram protein at 12 months versus 260 ± 10.03 nmoles Ca^{2+} per milligram protein at 3 months; **Fig. 3a**). mAPP mitochondria showed an even poorer calcium capacity compared to the nontransgenic mitochondria; impaired Ca^{2+} uptake capacity started at 6 months and progressively decreased in 12-month-old mAPP mice (reduction of 18% (220 ± 10.79 nmoles Ca^{2+} per milligram protein) and 50% (133.3 ± 16.67 nmoles Ca^{2+} per milligram protein) for 6 and 12 months, respectively, versus 3-month-old mAPP mice (267 ± 16.67 nmoles Ca^{2+} per milligram protein); **Fig. 3a**). Notably, mAPP-*Ppif*$^{-/-}$ cortical mitochondria were able to take up more Ca^{2+} (591.7 ± 11.1 nmoles Ca^{2+} per milligram protein and 333.3 ± 10.5 nmoles Ca^{2+} per milligram protein for 6 and 12 months, respectively) than mAPP mitochondria. Similarly, the addition of cyclosporine A, an inhibitor of CypD, to mAPP cortical mitochondria showed a higher buffering capacity of Ca^{2+} (**Fig. 3b**,**c**). Nontransgenic cortical mitochondria buffered against $CaCl_2$ uptake (242.9 ± 13 nmoles Ca^{2+} per milligram protein), and this capacity was significantly increased after preincubation with cyclosporine A (**Supplementary Fig. 4a**,**b** online). The *Ppif*$^{-/-}$ cortical mitochondria took up $CaCl_2$ (900 ± 25.8 nmoles Ca^{2+} per milligram protein) with a similar capacity to the cyclosporine A–treated nontransgenic mitochondria (**Supplementary Fig. 4a**,**b**).

To determine the function of the mPTP, we measured mitochondrial swelling in response to Ca^{2+}. Cortical mitochondria from transgenic and nontransgenic mice showed swelling in response to Ca^{2+}, and mAPP mitochondria showed a greater swelling at 12 months of age than did nontransgenic mitochondria, though cortical mitochondria of both nontransgenic and mAPP mice showed an age-dependent increase in swelling in response to Ca^{2+} (**Fig. 3d**,**e**). Notably, mAPP-*Ppif*$^{-/-}$ cortical mitochondria were more resistant to swelling and permeability transition induced by Ca^{2+} than were mAPP mitochondria (**Fig. 3d**,**f**). The addition of cyclosporine A to mAPP mitochondria also attenuated swelling in response to Ca^{2+} (**Fig. 3d**,**f**).

To assess the inner mitochondrial membrane potential in brain *in situ*, we loaded brain slices from transgenic mice with tetramethylrhodamine methyl ester (TMRM), a fluorescent probe to monitor the mitochondrial membrane potential. This indicator dye is a lipophilic cation accumulated by mitochondria in proportion to the membrane potential. Mitochondrial depolarization (disrupting or decreasing membrane potential) results in a loss of dye from the mitochondria and a decrease in mitochondrial fluorescence intensity. The intensity of TMRM staining was significantly decreased in the cerebral cortex and hippocampus of mAPP mice compared to other groups of mice (**Fig. 3g**). However, mAPP-*Ppif*$^{-/-}$ mice had mitochondria that were largely resistant to the loss of inner membrane potential, showing higher TMRM staining intensity than mAPP mice (**Fig. 3g**). Thus, mitochondria lacking CypD were protected from Aβ-mediated swelling and opening of the membrane permeability transition pore.

To evaluate mitochondrial reactive oxygen species (ROS) generation, we gave transgenic mice MitoSox Red, a unique fluorogenic dye used for highly selective detection of superoxide production in the mitochondria of live cells. The percentage of area occupied by MitoSox Red staining was considerably increased in the cerebral cortices and hippocampi (hippocampal regions CA1 to CA3) of mAPP mice by two- to threefold compared to other groups of mice, whereas mAPP-*Ppif*$^{-/-}$ mice showed much less MitoSox staining (**Fig. 4a** and **Supplementary Fig. 4c**,**d**). These data indicate that the absence of CypD attenuates Aβ-mediated mitochondrial ROS generation.

Further, mAPP mice showed an age-dependent increase in CypD translocation to the mitochondrial inner membrane (**Fig. 4b**). The CypD-Aβ complex was also present in the mitochondrial inner membrane of mAPP mice (**Fig. 4c**).

Next, we assessed mitochondrial function by measuring oxygen consumption, the activity of cytochrome *c* oxidase (COX IV) and ATP abundance in transgenic mouse brains. Compared to *Ppif*$^{-/-}$ and nontransgenic mice, mAPP mice showed a reduction in ADP-induced respiration control rate (RCR) at 6 and 12 months of age, whereas mAPP-*Ppif*$^{-/-}$ mice had a diminished reduction in RCR (**Fig. 4d**). Because mitochondria from mAPP mice had an impaired calcium capacity, we determined the effect of calcium on RCR. Calcium-induced RCR was decreased in 12-month-old mAPP cortical mitochondria but not in mAPP-*Ppif*$^{-/-}$ mitochondria as compared with

nontransgenic mitochondria (**Fig. 4e**). Additionally, mAPP mice had a reduced COX IV activity (**Fig. 4f**) and ATP abundance (**Fig. 4g**), whereas mAPP-*Ppif*$^{-/-}$ mice had markedly increased mitochondrial enzyme activity and ATP abundance (**Fig. 4f,g**). The COX IV activity and ATP abundance in nontransgenic mice were comparable to those in the *Ppif*$^{-/-}$ mice (**Fig. 4f,g**). Similarly, CypD-deficient mitochondria were also resistant to exogenous Aβ-mediated impairment in calcium capacity, swelling, CypD translocation and cytochrome *c* release (**Supplementary Fig. 5** online). These data indicate that CypD deficiency attenuates or protects against Aβ-mediated mitochondrial dysfunction.

CypD-Aβ interaction induces neuronal death

To directly determine the effects of CypD deficiency on Aβ- and oxidative stress–induced neuronal death, we examined cultured cortical neurons from nontransgenic and *Ppif*$^{-/-}$ mice (**Supplementary Fig. 6a** online). The CypD-Aβ complex was detected in nontransgenic cortical neurons but not in *Ppif*$^{-/-}$ neurons exposed to Aβ (**Supplementary Fig. 6b**). Incubation of Aβ42 with nontransgenic cortical neurons reduced mitochondrial membrane potential, as shown by TMRM staining, in a time- and dose-dependent manner, whereas *Ppif*$^{-/-}$ neurons had attenuated Aβ-induced reduction of the mitochondrial membrane potential (**Fig. 5a,b**). Consequently, Aβ-treated nontransgenic cortical neurons showed increased cytochrome *c* release as compared to Aβ-treated *Ppif*$^{-/-}$ and vehicle-treated neurons (**Fig. 5c**). The addition of carbonyl cyanide *p*-(trifluoromethoxy) phenylhydrazone (FCCP), a mitochondrial uncoupler, dissipated membrane potential and increased cytochrome *c* release in nontransgenic and *Ppif*$^{-/-}$ neurons. The absence of CypD attenuated Aβ-induced apoptosis, as shown by a reduction in the

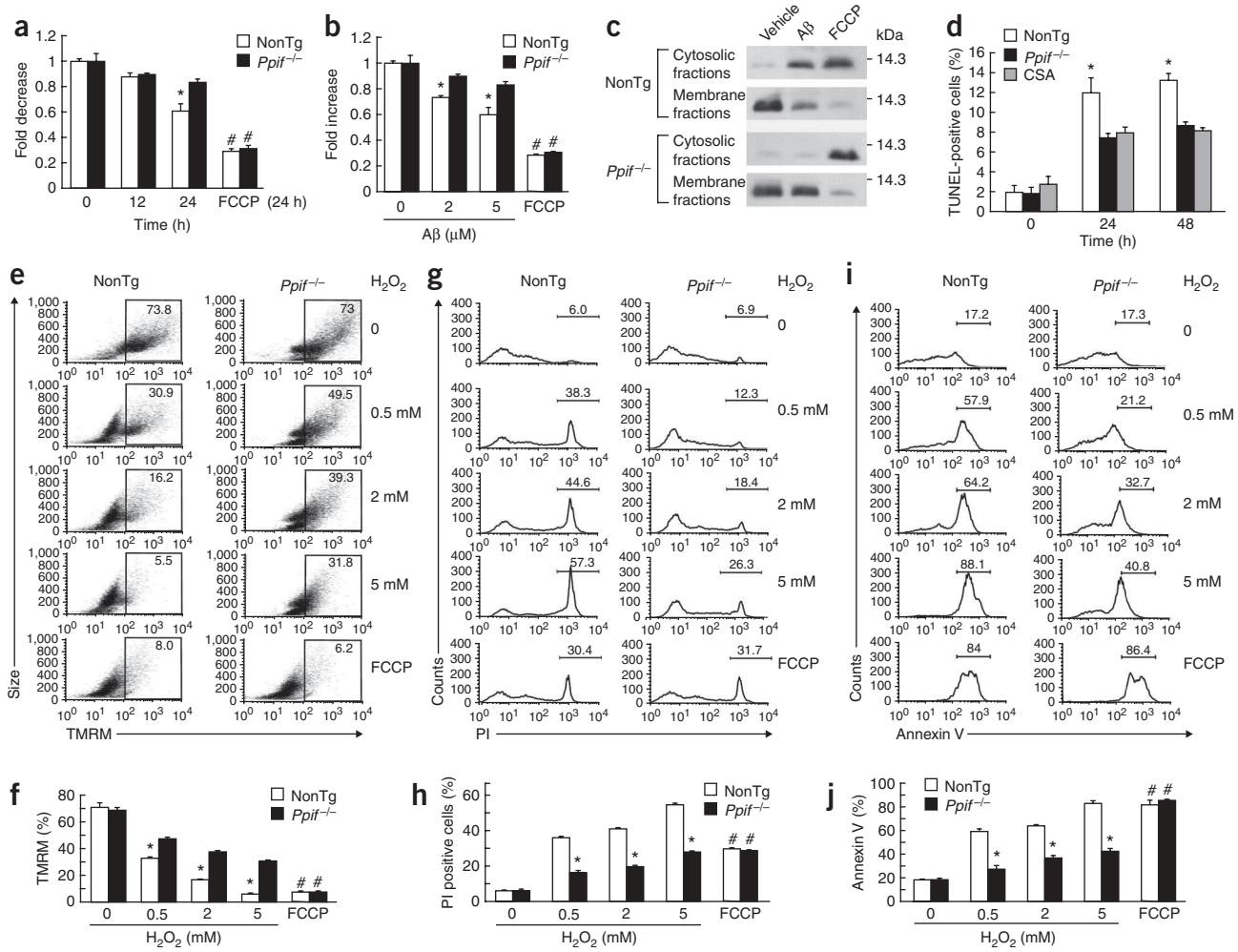

Figure 5 Aβ- and H_2O_2-induced mitochondrial and neuronal dysfunction in cultured neurons. (**a**,**b**) Fluorescence intensity of TMRM in cultured neurons treated with 5 μM Aβ42 at either the indicated times (**a**) or the indicated doses of Aβ42 given for 24 h (**b**). $^{*}P < 0.01$ versus Aβ-treated *Ppif*$^{-/-}$ neurons. $^{\#}P < 0.001$ in FCCP-treated (5 μM) neurons compared to other groups of neurons. (**c**) Immunoblotting for cytochrome *c* in cytosolic and membrane fractions from nontransgenic and *Ppif*$^{-/-}$ cultured cortical neurons treated with Aβ (2 μM) or FCCP (5 μM) for 24 h. (**d**) The percentage of TUNEL-positive neurons quantified in nonTg and *Ppif*$^{-/-}$ neurons treated with Aβ (2 μM) or Aβ plus CSA (1 μM) for the indicated times. (**e**–**j**) Effect of CypD on H_2O_2-induced cell death. (**e**–**f**) Mitochondrial inner membrane potential changes. NonTg and *Ppif*$^{-/-}$ neurons were treated with increasing concentrations of H_2O_2 for one hour and then analyzed by FACS for TMRM staining. (**e**) Representative FACS analysis of TMRM-positive cells. (**f**,**h**,**j**) The percentage of TMRM- (**f**), propidium iodide (PI)- (**h**) and annexin V– (**j**) positive cells combined from three or four independent experiments. $^{*}P < 0.001$ versus vehicle-treated neurons or H_2O_2-treated *Ppif*$^{-/-}$ neurons. $^{\#}P < 0.01$ versus vehicle-treated neurons. (**g**–**j**) FACS analysis of PI (**g**,**h**) and annexin V (**i**,**j**) staining in nontransgenic and *Ppif*$^{-/-}$ neurons treated with H_2O_2 for one hour. The percentage of PI- or annexin V–positive cells is indicated as number with underline. Representative histograms for FACS analysis of PI (**g**) and Annexin V (**i**).

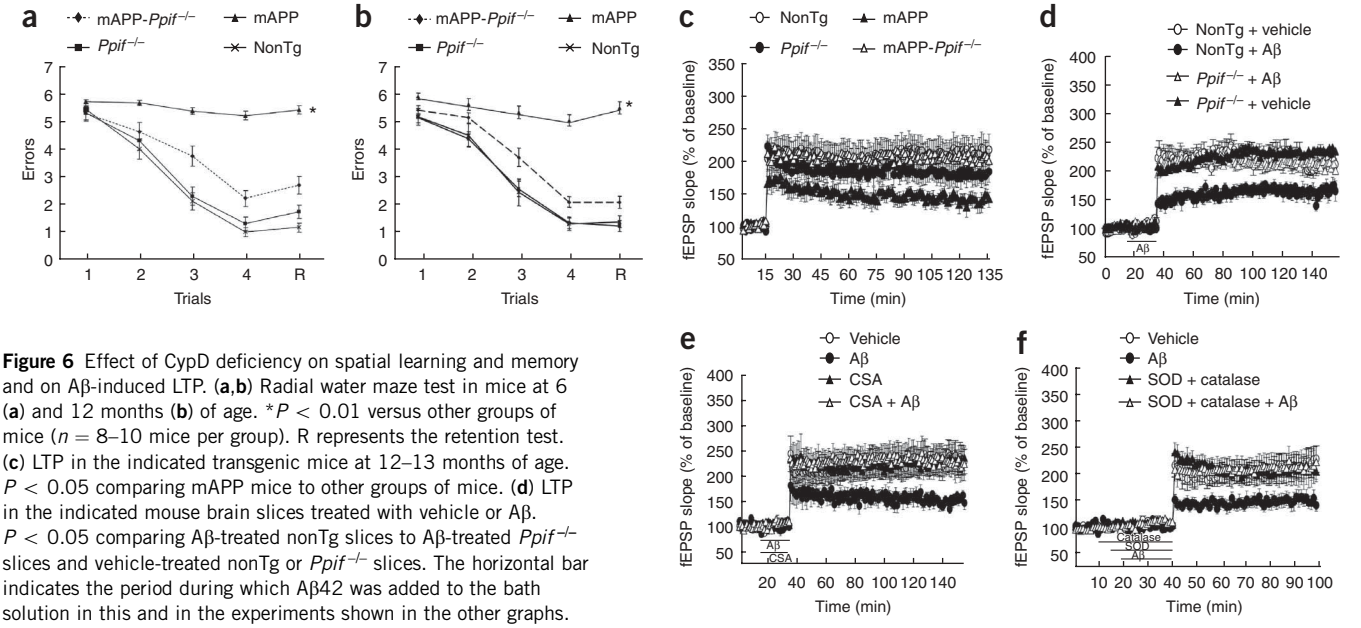

Figure 6 Effect of CypD deficiency on spatial learning and memory and on Aβ-induced LTP. (**a**,**b**) Radial water maze test in mice at 6 (**a**) and 12 months (**b**) of age. $*P < 0.01$ versus other groups of mice ($n = 8$–10 mice per group). R represents the retention test. (**c**) LTP in the indicated transgenic mice at 12–13 months of age. $P < 0.05$ comparing mAPP mice to other groups of mice. (**d**) LTP in the indicated mouse brain slices treated with vehicle or Aβ. $P < 0.05$ comparing Aβ-treated nonTg slices to Aβ-treated *Ppif*$^{-/-}$ slices and vehicle-treated nonTg or *Ppif*$^{-/-}$ slices. The horizontal bar indicates the period during which Aβ42 was added to the bath solution in this and in the experiments shown in the other graphs. (**e**) Effect of CSA (1 μM) on Aβ-induced LTP in nonTg hippocamal slices. $P < 0.05$ comparing Aβ-induced LTP to LTP in the slices treated with CSA plus Aβ, vehicle or CSA alone. $P > 0.05$ comparing CSA alone to vehicle-treated slices. (**f**) Effect of scavenging superoxide through perfusion with SOD (100 U ml^{-1}) plus catalase (260 U ml^{-1}) on Aβ-induced LTP in nonTg hippocampal slice. $P < 0.05$ comparing Aβ-treated slices to the slices treated with SOD + catalase + Aβ or with vehicle. $P > 0.05$ comparing vehicle-treated slices to the slices treated with SOD and catalase alone.

number of TUNEL-positive cells in *Ppif*$^{-/-}$ neurons exposed to Aβ (**Fig. 5d**). The addition of cyclosporine A had a similar effect on Aβ-induced apoptosis (**Fig. 5d**).

Because CypD deficiency attenuated ROS generation (**Fig. 4a**) in mAPP mice, we evaluated the direct effect of CypD deficiency on oxidative stress–induced mitochondrial and neuronal toxicity. Flow cytometry analysis of fluorescently labeled cells showed a marked dose-dependent reduction in the number of TMRM-positive cells in both nontransgenic and *Ppif*$^{-/-}$ neurons exposed to increasing concentrations of H_2O_2. However, *Ppif*$^{-/-}$ neurons were more resistant to H_2O_2-induced loss of membrane potential than were nontransgenic neurons, as shown by a higher percentage of TMRM-positive cells amongst H_2O_2-treated *Ppif*$^{-/-}$ neurons (31.8%) compared to H_2O_2-treated nontransgenic neurons (5.5%; **Fig. 5e**,**f**). A protective effect of CypD deficiency on H_2O_2-mediated reduction in membrane potential was further evaluated by measuring the percentage of TMRM-labeled living cells with fluorescent microscopy (**Supplementary Fig. 6c**). FACS analysis revealed significant increases in propidium iodide– (**Fig. 5g**,**h**) and annexin V– (**Fig. 5i**,**j**) positive cells after H_2O_2 treatment in nontransgenic neurons, whereas *Ppif*$^{-/-}$ neurons were protected from H_2O_2-induced cell death (**Fig. 5g–j**).

CypD deficiency improves behavioral and synaptic function

The radial arm water maze test was used to assess the spatial learning and memory of transgenic mice. At 6 and 12 months of age, *Ppif*$^{-/-}$ and nontransgenic mice showed a strong learning and memory capacity (**Fig. 6a**,**b**), whereas mAPP mice showed impaired spatial learning and memory for the platform location during trial 4 and retention test (average of about five or six errors by trial 4 and the retention test). The mAPP-*Ppif*$^{-/-}$ mice had substantially improved spatial learning and memory (approximately two or three errors by trial 4 and the retention test; **Fig. 6a**,**b**), indicating that the absence of CypD improves learning and memory in mice with Alzheimer's-like disease.

Given that mAPP-*Ppif*$^{-/-}$ mice showed an improvement in learning and memory, we examined whether these mice also had an improvement in long-term potentiation (LTP), a form of synaptic plasticity that is widely studied as a cellular model for learning and memory. Slices from 12–13-month-old mAPP mice showed a reduction in LTP compared to slices from nontransgenic littermates (140.99 ± 11.81% at 120 min after the tetanus versus 218.52 ± 24.38%; $n = 10$–12, $P < 0.05$; **Fig. 6c**). Slices from mAPP-*Ppif*$^{-/-}$ littermates, in turn, showed normal LTP (199.32 ± 20.01%; $n = 13$, $P < 0.05$ compared to mAPP mice and $P > 0.05$ compared to nontransgenic mice; **Fig. 6c**) and improved basal synaptic transmission compared to mAPP slices (**Supplementary Fig. 6d**). The *Ppif*$^{-/-}$ slices also showed a normal LTP (184.70 ± 16.47%; $n = 10$, $P > 0.05$ compared to nontransgenic slices). To test a direct effect of CypD deficiency on Aβ-mediated reduction of LTP, we recorded LTP in hippocampal slices from *Ppif*$^{-/-}$ and nontransgenic mice treated with Aβ. We found similar amounts of potentiation in CypD-deficient slices compared to nontransgenic slices in the presence of vehicle (230.06 ± 24.71% versus 209.39 ± 15.77%, $n = 6$ or 7, $P > 0.05$; **Fig. 6d**). However, CypD deficiency protected hippocampal slices against a reduction of LTP by 200 nM oligomeric Aβ42 (206.42 ± 17.35% in Aβ-treated *Ppif*$^{-/-}$ slices versus 163.91 ± 17.36% in Aβ-treated nontransgenic slices; $n = 7$–9, $P < 0.05$; **Fig. 6d**). Basal synaptic transmission was not affected in the *Ppif*$^{-/-}$ mice. The addition of cyclosporine A (1 μM) rescued Aβ-induced reduction of LTP in nontransgenic hippocampal slices (219.61 ± 30.27% after treatment with cyclosporine A and Aβ versus 145.96 ± 13.09% after Aβ treatment; $n = 7$ or 8, $P < 0.05$; **Fig. 6e**). Cyclosporine A alone did not alter LTP (232.43 ± 23.19% in cyclosporine A–treated slices versus 227.57 ± 24.16% in vehicle-treated nontransgenic slices; $n = 6$ or 7, $P > 0.05$; **Fig. 6e**). These results confirm previous data showing that Aβ impairs LTP[38]. Most notably, they indicate that CypD deficiency may protect against the deleterious effects of Aβ soluble oligomers on synaptic function.

We next determined whether Aβ-mediated reduction of LTP can be prevented by ROS scavenging. The addition of 100 U ml^{-1} superoxide dismutase (SOD, a scavenger of superoxide, converting it into oxygen and hydrogen peroxide) plus 260 U ml^{-1} catalase (to prevent inhibition of LTP by H_2O_2 through its conversion into oxygen and water[39,40]) blocked Aβ-induced inhibition of LTP in nontransgenic hippocampal slices (220.89 ± 30.97% in SOD-, catalase- and Aβ-treated slices versus 145.37 ± 12.24% in Aβ alone–treated nontransgenic slices; $n = 7$ or 8, $P < 0.05$; **Fig. 6f**). SOD plus catalase did not alter LTP (205.05 ± 11.79% in SOD- and catalase-treated slices versus 219.30 ± 24.42% in vehicle-treated nontransgenic slices; $n = 6$–8, $P > 0.05$; **Fig. 6f**). These experiments suggest a role for ROS in Aβ-mediated impairment of LTP.

DISCUSSION

Our data show that the expression of CypD is associated with amyloid pathology and aging in the brain. The increased expression of CypD could be an explanation for the observed aging- and Aβ-related impairment of mitochondrial function, as CypD is a key component of the mPTP, and its abundance is associated with the vulnerability of the mPTP to Ca^{2+} (refs. 41,42). Our studies indicate that the genetic removal of this Aβ binding partner, within Aβ-containing mitochondria, improves mitochondrial, neuronal and synaptic function. Therefore, it will be useful to understand the structural basis of the CypD-Aβ interaction, and further investigation by crystallization and mutational analysis is required to identify the amino acid sequences of CypD responsible for its binding to Aβ.

Although Aβ can directly disrupt mitochondrial function and cause oxidative stress[18,43,44], the interaction of mitochondrial Aβ with CypD significantly enhances the accumulation and production of mitochondrial ROS, which is a strong inducer for the recruitment of CypD to the mitochondrial inner membrane. In addition, other stimuli such as ROS, directly produced by Aβ itself or by the interaction of Aβ with mitochondrial amyloid-binding alcohol dehydrogenase[8,9], could result in CypD recruitment, leading to mPTP opening, loss of membrane potential and, eventually, cell death. The excessive ROS will exaggerate oxidative damage and mitochondrial malfunction, including the collapse of the membrane potential[9,45,46]. This is evident in CypD-deficient mAPP mice, which had a reduction in the accumulation of mitochondrial ROS in conjunction with a higher mitochondrial polarization.

Finally, deficiency of CypD significantly improved cognitive and synaptic function in a mouse model of Alzheimer's disease. The addition of ROS-scavenging enzymes alleviated Aβ-mediated reduction of LTP. These results, combined with the evidence that lack of CypD attenuated ROS generation and protected neurons from Aβ- and oxidative stress–induced injury, indicate that oxidative damage induced by the CypD-Aβ interaction may be a mechanism underlying the impairments in synaptic plasticity and memory in Alzheimer's disease[47–49]. Mitochondria can also become severely dysfunctional through the permeability transition induced by the synergistic effects of oxidative stress and dysregulation of cytosolic free Ca^{2+}. Therefore, synaptic and memory dysfunction mediated by Aβ binding to CypD may involve other mechanisms such as Ca^{2+}-regulated signaling pathways, oxidative stress–mediated kinase systems and activation of transcription factors[38,50–53]. Further investigations are required to elucidate these alternative mechanisms.

Taken together, our studies have clearly shown that CypD and Aβ directly interact with each other in the mitochondria of Alzheimer's disease brain and in a transgenic mouse model of Alzheimer's disease. This CypD-Aβ interaction promotes ROS generation and CypD recruitment to the mitochondrial inner membrane, leading to the formation of the mPTP. CypD-mediated mPTP formation has a crucial role in regulating mitochondrial-induced cell death in an Aβ-rich environment, although the openings in the outer mitochondrial membrane associated with activation of members of the Bcl-2 family, either proapoptotic (Bax, BAD and Bak among others) or antiapoptotic (Bcl-2, Bcl-xL and Bcl-w, among others) proteins (such as the accumulation of Bax at the outer mitochondrial membrane induced by intracellular Aβ), may also contribute to neurotoxicity[54]. Our studies provide new insights into the mechanism underlying Aβ-mediated mitochondrial stress through an interaction with CypD. The absence of CypD protects neurons from Aβ- and oxidative stress–induced cell death, impaired learning and memory and synaptic dysfunction. Therefore, CypD is a key mitochondrial target for Aβ-induced mitochondrial and synaptic dysfunction. Blockade of CypD may be a potential therapeutic approach for halting Alzheimer's disease.

METHODS

Mice. Mouse studies were approved by the Animal Care and Use Committee of Columbia University in accordance with the US National Institutes of Health guidelines for animal care. We crossed transgenic mice overexpressing a mutant human form of amyloid precursor protein (mAPP, J-20 line)[9,50] with *Ppif*$^{-/-}$ mice[30] to generate CypD-deficient mAPP mice (mAPP-*Ppif*$^{-/-}$).

Human tissues. We obtained human brain tissues of temporal cortex (temporal pole, including Brodmann area 38, which is the apparent rostral origin of the superior, middle and inferior temporal gyri) and hippocampus from individuals with Alzheimer's disease and age-matched, non–Alzheimer's disease controls from New York Brain Bank at Columbia University. Detailed information for each of the cases studied is shown in **Supplementary Table 1** online. We obtained informed consent from all subjects. The study was approved by the Institutional Review Board of Columbia University.

Isolation of mitochondria. We isolated mitochondria from the cortices of Alzheimer's disease brains or cortices of mouse brains as previously described[6,9]. We used the highly purified mitochondria for immunoblotting and immunoprecipitation. For the mitochondrial function assay, mitochondria were isolated by centrifuging brain homogenates at 1,500*g* for 5 min at 4 °C. We adjusted the supernatant to 10% Percoll and recentrifuged at 12,000*g* for 10 min. We resuspended the mitochondrial pellet in the isolation buffer (225 mM D-mannitol, 75 mM sucrose, 2 mM K_2HPO_4, 5 mM HEPES, pH 7.2) containing 0.01% digitonin and recentrifuged at 6,000*g* for 10 min. We isolated cell mitochondria with a mitochondrial fractionation kit (Active Motif). We determined protein concentration by the Bio-Rad DC protein assay (BioRad).

Immunoblotting analysis. We subjected mitochondrial proteins to immunoblotting with antibody to CypD (1 μg ml^{-1}, generated in our laboratory) followed by goat antibody to rabbit IgG conjugated with peroxidase to determine the expression level of CypD. We used chemiluminescent substrate (Roche) to detect the CypD immunoreactive band. We reprobed the membrane with antibody to COX IV (to human COX IV, Invitrogen; or to mouse COX IV, Abcam).

Immunoprecipitation and immunoblotting for detection of CypD-Aβ complex. We resuspended mitochondria from cerebral cortices of transgenic mice or human subjects in buffer (500 μg ml^{-1}, 50 mM Tris, 150 mM NaCl, 1 mM EDTA, protease inhibitors (Calbiochem, set V, EDTA free), 0.1% NP-40, pH 7.5) and subjected them to five freeze-thaw cycles, followed by centrifugation at 14,000*g* for 5 min at 4 °C. We immunoprecipitated the resulting supernatant with rabbit antibody to CypD (1:500 dilution) at 4 °C overnight, followed by a second incubation with protein A/G (Pierce) for 2 h at 20 °C. We subjected the resultant immunoprecipitant to immunoblotting with antibody to Aβ (6E10,1:3,000, Signat).

Surface plasmon resonance study of CypD-Aβ interaction. See **Supplementary Methods** online.

Immunostaining for confocal and electron microscopy study. See **Supplementary Methods** online.

Mitochondrial function assays. We monitored mitochondrial oxygen consumption with a Clark oxygen electrode (Oxytherm, Hansatech) as previously described[6].

We performed the mitochondrial swelling assay according to a previously published method[34] with modifications (**Supplementary Methods**).

We measured mitochondrial calcium retention capacity with the fluorescent indicator Calcium Green 5N (Invitrogen). We suspended mitochondria (100 μg) at 20 °C in 1 ml respiration buffer (150mM KCl, 5mM HEPES, 2mM K_2HPO_4, pH 7.2) containing 1 μM Calcium Green 5N with pulsate injection of calcium into the cuvette. We monitored fluorescence with an excitation of 506 nm and an emission of 531 nm with a FluoroMax-2 spectrophotometer (Jobin Yvon-Spex Instruments).

We measured cytochrome *c* release, activity of COX IV and ATP abundance in brain as described in the **Supplementary Methods**.

***In situ* detection of mitochondrial reactive oxygen species and membrane potential.** We performed *in situ* measurements of ROS in brain slices as previously described[55] with modifications. We injected MitoSox Red (1mg kg^{-1}, Invitrogen) intravenously via the tail vein. After 30 min, we anesthetized the mice with ketamine (100 mg kg^{-1}) and xylazine (10 mg kg^{-1}) and killed them by transcardial perfusion with cold saline (5 min) and then cold, freshly prepared 3.7% paraformaldehyde (3 min). We quickly removed the brain and froze it in 2-methyl butane with dry ice. We immediately cut coronal frozen brain sections (6 μm) and mounted them with DAPI-containing mounting medium (Vector Laboratories). We examined sections under a fluorescence microscope immediately after the mounting. We analyzed the area occupied by MitoSox Red staining with the Universal image program. Brain sections from mice were blindly coded and processed in parallel. Codes were broken after the analysis was complete.

For evaluation of membrane potential, we perfused anesthetized mice with cold saline for 3 min. We incubated frozen brain sections with TMRM (50 nM, Invitrogen) in PBS for 15 min. We quantified the intensity of TMRM staining with the Universal image program.

CypD translocation. We examined CypD translocation to the inner membrane as previously described[28,56] (**Supplementary Methods**).

Determination of cytochrome *c* release, membrane potential and apoptosis in cultured neurons. We incubated primary cultured neurons with Aβ (2–5 μM) for 12–24 h or with H_2O_2 (0.5, 2 and 5 mM) for 1 h and then treated them with TMRM (100 nM) for 30 min. We observed the cells under a microscope or trypsinized them for detection of TMRM by flow cytometry (Becton Dickinson FACS Calibur). We analyzed flow cytometric data by Flowjo 7 (Tree Star).

We assessed cytochrome *c* release by immunoblotting with antibody to cytochrome *c* (Invitrogen). We determined apoptosis by detecting TUNEL-positive cells using an *in situ* cell death detection kit (Roche). We analyzed propidium iodide– or annexin V–labeled cells by flow cytometry.

Behavioral and electrophysiological studies. We performed behavioral studies to assess spatial learning and memory in the radial arm water maze as previously described[9,50]. We performed the retention tests 30 min after the fourth test. The four groups of mice in the behavioral studies were littermates and gender-matched to enhance the reproducibility and reliability of our results in the radial arm water maze. Investigators were unaware of mouse genotypes until the behavioral tests were finished.

We performed electrophysiological recordings on transverse hippocampal slices (400 μm in thickness) as previously described[38] (**Supplementary Methods**).

Statistical analyses. We performed statistical analyses with Student's *t*-test and one-way analysis of variance using the Statview statistics software. $P < 0.05$ was considered significant. All data are expressed as means ± s.e.m.

Note: Supplementary information is available on the Nature Medicine website.

ACKNOWLEDGMENTS

This work was supported by the US Public Health Service Commissioned Corps (PO1 AG17490, PO50 AG08702) and the Alzheimer's Association. We thank S. Katz for assistance with performing the behavioral experiments.

AUTHOR CONTRIBUTIONS

H.D. designed and did experiments and assisted with the preparation of the manuscript. L.G. contributed to the study of *in vitro* cultured neurons. F.F. did quantitative real-time PCR experiments. L.G. and D.C. performed genotyping of transgenic mice. A.A.S. and G.M.M. conducted electron microscopy studies. Y.Y. and C.W. performed surface plasmon resonance experiments. F.J.G.-M. provided some suggestions. J.D.M. provided CypD-knockout mice. H.Z. and O.A. performed LTP experiments. J.P.V. provided information of human brain tissues. J.X.C. provided suggestions for the experimental design and assisted with the preparation of manuscript. S.D.Y. initiated, directed and supervised the research, designed and assisted experiments, analyzed data, developed the concept and wrote the manuscript.

Published online at http://www.nature.com/naturemedicine/
Reprints and permissions information is available online at http://npg.nature.com/reprintsandpermissions/

1. Mauren, I., Zierz, S. & Moller, H.J. A selective defect of cytochrome *c* oxidase is present in brain of Alzheimer disease patients. *Neurobiol. Aging* **21**, 455–462 (2000).
2. Blass, J.P. The mitochondrial spiral. An adequate cause of dementia in the Alzheimer's syndrome. *Ann. NY Acad. Sci.* **924**, 170–183 (2000).
3. Sheehan, J.P. *et al.* Calcium homeostasis and reactive oxygen species production in cells transformed by mitochondria from individuals with sporadic Alzheimer's disease. *J. Neurosci.* **17**, 4612–4622 (1997).
4. Cardoso, S.M., Santana, I., Swerdlow, R.H. & Oliveira, C.R. Mitochondria dysfunction of Alzheimer's disease cybrids enhances Aβ toxicity. *J. Neurochem.* **89**, 1417–1426 (2004).
5. Lin, M.T. & Beal, M.F. Alzheimer's APP mangles mitochondria. *Nat. Med.* **12**, 1241–1243 (2006).
6. Caspersen, C. *et al.* Mitochondrial Aβ: a potential focal point for neuronal metabolic dysfunction in Alzheimer's disease. *FASEB J.* **19**, 2040–2041 (2005).
7. Manczak, M. *et al.* Mitochondria are a direct site of Aβ accumulation in Alzheimer's disease neurons: implications for free radical generation and oxidative damage in disease progression. *Hum. Mol. Genet.* **15**, 1437–1449 (2006).
8. Takuma, K. *et al.* ABAD enhances Aβ-induced cell stress via mitochondrial dysfunction. *FASEB J.* **19**, 597–598 (2005).
9. Lustbader, J.W. *et al.* ABAD directly links Aβ to mitochondrial toxicity in Alzheimer's disease. *Science* **304**, 448–452 (2004).
10. Reddy, P.H. Amyloid precursor protein–mediated free radicals and oxidative damage: implications for the development and progression of Alzheimer's disease. *J. Neurochem.* **96**, 1–13 (2006).
11. Wang, J. *et al.* Hepatitis C virus non-structural protein NS5A interacts with FKBP38 and inhibits apoptosis in Huh7 hepatoma cells. *FEBS Lett.* **580**, 4392–4400 (2006).
12. Shukkur, E.A. *et al.* Mitochondrial dysfunction and tau hyperphosphorylation in Ts1Cje, a mouse model for Down syndrome. *Hum. Mol. Genet.* **15**, 2752–2762 (2006).
13. Hirai, K. *et al.* Mitochondrial abnormalities in Alzheimer's disease. *J. Neurosci.* **21**, 3017–3023 (2001).
14. Crouch, P.J. *et al.* Copper-dependent inhibition of human cytochrome *c* oxidase by a dimeric conformer of amyloid-β1–42. *J. Neurosci.* **25**, 672–679 (2005).
15. Devi, L., Prabhu, B.M., Galati, D.F., Avadhani, N.G. & Anandatheerthavarada, H.K. Accumulation of amyloid precursor protein in the mitochondrial import channels of human Alzheimer's disease brain is associated with mitochondrial dysfunction. *J. Neurosci.* **26**, 9057–9068 (2006).
16. Fernandez-Vizarra, P. *et al.* Intra- and extracellular Aβ and PHF in clinically evaluated cases of Alzheimer's disease. *Histol. Histopathol.* **19**, 823–844 (2004).
17. Chen, X., Stern, D. & Yan, S.D. in *Neurobiology of Alzheimer's Disease* (eds. Dawbarn, D. & Allen, S.J.) 227–244 (Oxford University Press, Oxford, 2007).
18. Cardoso, S.M., Santos, S., Swerdlow, R.H. & Oliveira, C.R. Functional mitochondria are required for amyloid β–mediated neurotoxicity. *FASEB J.* **15**, 1439–1441 (2001).
19. Crompton, M. Mitochondria and aging: a role for the permeability transition? *Aging Cell* **3**, 3–6 (2004).
20. Halestrap, A.P., McStay, G.P. & Clarke, S.J. The permeability transition pore complex: another view. *Biochimie* **84**, 153–166 (2002).
21. Halestrap, A. Biochemistry: a pore way to die. *Nature* **434**, 578–579 (2005).
22. Zamzami, N., Larochette, N. & Kroemer, G. Mitochondrial permeability transition in apoptosis and necrosis. *Cell Death Differ.* **12** Suppl 2, 1478–1480 (2005).
23. Crompton, M., Barksby, E., Johnson, N. & Capano, M. Mitochondrial intermembrane junctional complexes and their involvement in cell death. *Biochimie* **84**, 143–152 (2002).
24. Halestrap, A.P. Calcium, mitochondria and reperfusion injury: a pore way to die. *Biochem. Soc. Trans.* **34**, 232–237 (2006).

25. Bernardi, P. *et al.* The mitochondrial permeability transition from in vitro artifact to disease target. *FEBS J.* **273**, 2077–2099 (2006).
26. Crompton, M., Virji, S. & Ward, J.M. Cyclophilin-D binds strongly to complexes of the voltage-dependent anion channel and the adenine nucleotide translocase to form the permeability transition pore. *Eur. J. Biochem.* **258**, 729–735 (1998).
27. Halestrap, A.P., Woodfield, K.Y. & Connern, C.P. Oxidative stress, thiol reagents, and membrane potential modulate the mitochondrial permeability transition by affecting nucleotide binding to the adenine nucleotide translocase. *J. Biol. Chem.* **272**, 3346–3354 (1997).
28. Connern, C.P. & Halestrap, A.P. Recruitment of mitochondrial cyclophilin to the mitochondrial inner membrane under conditions of oxidative stress that enhance the opening of a calcium-sensitive non-specific channel. *Biochem. J.* **302**, 321–324 (1994).
29. Andreeva, L., Heads, R. & Green, C.J. Cyclophilins and their possible role in the stress response. *Int. J. Exp. Pathol.* **80**, 305–315 (1999).
30. Baines, C.P. *et al.* Loss of cyclophilin D reveals a critical role for mitochondrial permeability transition in cell death. *Nature* **434**, 658–662 (2005).
31. Pastorino, J.G., Chen, S.T., Tafani, M., Snyder, J.W. & Farber, J.L. The overexpression of Bax produces cell death upon induction of the mitochondrial permeability transition. *J. Biol. Chem.* **273**, 7770–7775 (1998).
32. Nakagawa, T. *et al.* Cyclophilin D–dependent mitochondrial permeability transition regulates some necrotic but not apoptotic cell death. *Nature* **434**, 652–658 (2005).
33. Basso, E. *et al.* Properties of the permeability transition pore in mitochondria devoid of cyclophilin D. *J. Biol. Chem.* **280**, 18558–18561 (2005).
34. Schinzel, A.C. *et al.* Cyclophilin D is a component of mitochondrial permeability transition and mediates neuronal cell death after focal cerebral ischemia. *Proc. Natl. Acad. Sci. USA* **102**, 12005–12010 (2005).
35. Yan, Y. *et al.* Surface plasmon resonance and nuclear magnetic resonance studies of ABAD-Aβ interaction. *Biochemistry* **46**, 1724–1731 (2007).
36. Aguilar, M.I. & Small, D.H. Surface plasmon resonance for the analysis of β-amyloid interactions and fibril formation in Alzheimer's disease research. *Neurotox. Res.* **7**, 17–27 (2005).
37. Bergersen, L.H., Storm-Mathisen, J. & Gundersen, V. Immunogold quantification of amino acids and proteins in complex subcellular compartments. *Nat. Protoc.* **3**, 144–152 (2008).
38. Vitolo, O.V. *et al.* Amyloid β-peptide inhibition of the PKA/CREB pathway and long-term potentiation: reversibility by drugs that enhance cAMP signaling. *Proc. Natl. Acad. Sci. USA* **99**, 13217–13221 (2002).
39. Klann, E., Roberson, E.D., Knapp, L.T. & Sweatt, J.D. A role for superoxide in protein kinase C activation and induction of long-term potentiation. *J. Biol. Chem.* **273**, 4516–4522 (1998).
40. Kamsler, A. & Segal, M. Paradoxical actions of hydrogen peroxide on long-term potentiation in transgenic superoxide dismutase-1 mice. *J. Neurosci.* **23**, 10359–10367 (2003).
41. Naga, K.K., Sullivan, P.G. & Geddes, J.W. High cyclophilin D content of synaptic mitochondria results in increased vulnerability to permeability transition. *J. Neurosci.* **27**, 7469–7475 (2007).
42. Eliseev, R.A. *et al.* Role of cyclophilin D in the resistance of brain mitochondria to the permeability transition. *Neurobiol. Aging* **28**, 1532–1542 (2007).
43. Morais Cardoso, S., Swerdlow, R.H. & Oliveira, C.R. Induction of cytochrome c-mediated apoptosis by amyloid β 25–35 requires functional mitochondria. *Brain Res.* **931**, 117–125 (2002).
44. Moreira, P.I., Santos, M.S., Moreno, A., Rego, A.C. & Oliveira, C. Effect of amyloid β-peptide on permeability transition pore: a comparative study. *J. Neurosci. Res.* **69**, 257–267 (2002).
45. Maragos, W.F. *et al.* Methamphetamine toxicity is attenuated in mice that overexpress human manganese superoxide dismutase. *Brain Res.* **878**, 218–222 (2000).
46. Hensley, K. *et al.* A model for β-amyloid aggregation and neurotoxicity based on free radical generation by the peptide: relevance to Alzheimer disease. *Proc. Natl. Acad. Sci. USA* **91**, 3270–3274 (1994).
47. Serrano, F. & Klann, E. Reactive oxygen species and synaptic plasticity in the aging hippocampus. *Ageing Res. Rev.* **3**, 431–443 (2004).
48. Liu, R. *et al.* Reversal of age-related learning deficits and brain oxidative stress in mice with superoxide dismutase/catalase mimetics. *Proc. Natl. Acad. Sci. USA* **100**, 8526–8531 (2003).
49. Esposito, L. *et al.* Reduction in mitochondrial superoxide dismutase modulates Alzheimer's disease-like pathology and accelerates the onset of behavioral changes in human amyloid precursor protein transgenic mice. *J. Neurosci.* **26**, 5167–5179 (2006).
50. Arancio, O. *et al.* RAGE potentiates Aβ-induced perturbation of neuronal function in transgenic mice. *EMBO J.* **23**, 4096–4105 (2004).
51. Yan, S.D. *et al.* RAGE and amyloid-β peptide neurotoxicity in Alzheimer's disease. *Nature* **382**, 685–691 (1996).
52. Xie, C.W. Calcium-regulated signaling pathways: role in amyloid β–induced synaptic dysfunction. *Neuromolecular Med.* **6**, 53–64 (2004).
53. Origlia, N. *et al.* Receptor for advanced glycation end product-dependent activation of p38 mitogen-activated protein kinase contributes to amyloid-β–mediated cortical synaptic dysfunction. *J. Neurosci.* **28**, 3521–3530 (2008).
54. Hou, F.F. *et al.* Receptor for advanced glycation end products on human synovial fibroblasts: role in the pathogenesis of dialysis-related amyloidosis. *J. Am. Soc. Nephrol.* **13**, 1296–1306 (2002).
55. Murakami, K. *et al.* Mitocondrial susceptibility to oxidative stress exacerbates cerebral infarction that follows permanent focal cerebral ischemia in mutant mice with manganese superoxide dismutase deficiency. *J. Neurosci.* **18**, 205–213 (1998).
56. Friberg, H., Connern, C., Halestrap, A.P. & Wieloch, T. Differences in the activation of the mitochondrial permeability transition among brain regions in the rat correlate with selective vulnerability. *J. Neurochem.* **72**, 2488–2497 (1999).